Structure-Dependent Electrochemical Behavior of Thienylplatinum(II) Complexes of N,N-Heterocycles

Feng Zhao,[a] Xingling Xu,[a] Soo Beng Khoo,*[a] and T. S. Andy Hor*[a]

Keywords: Platinum / N ligands / Cyclic voltammetry / Thin films / Heterocycles

trans-[Pt(MeCN)(PPh_3)$_2$(2-thienyl)]BF_4 (**1**) serves as a convenient precursor to bifunctional mononuclear *trans*-[Pt(PPh_3)$_2$(η^1-*N*-*N*)(2-thienyl)]BF_4 [*N*-*N* = pyrazine (**2**); 2-chloropyrazine, (**3**)] and dinuclear *trans,trans*-[Pt_2(PPh_3)$_4$(μ-*N*-*N*)(2-thienyl)$_2$](BF_4)$_2$ [(*N*-*N* = 4,4′-bipyridine (**4**); 4,4′-vinylenedipyridine (**5**)] complexes. The nuclear selectivity is conveniently controlled by the choice of the heterocyclic ligands or spacers. Both structural types **3** and **5** were confirmed by single-crystal X-ray crystallographic analyses. Their solution identities were established by positive-ion Electrospray Mass Spectrometry (ESMS). The electroactivities of these complexes were studied by cyclic voltammetry (CV). Continuous CV scans of **4** and **5** revealed variations in the redox waves with the number of scans. While the initial oxidative scan exhibited only a broad, irreversible wave, further cycling showed the growth of two additional redox couples up to about the tenth cycle. The peak currents of these redox couples began to decay with prolonged potential cycling beyond the tenth cycle. These findings are consistent with the formation of electroactive oligomers/polymers, and this conclusion is supported by visible thin film formation on the electrodes. In contrast, the mononuclear complexes (**2** and **3**) do not show such behavior. The films formed were further studied by repetitive potential cycling and XPS.

Introduction

The preparation of macro- and supramolecular assemblies with functionalised properties is currently a major challenge in synthetic chemistry.[1] A careful selection of a transition metal and a conjugated ligand could result in not only targeted molecular sizes and shapes,[2] but also expected electrochemical, magnetic and optical properties. Incorporation of transition metals into the conjugated backbone enhances metal dπ-pπ* back-bonding, which is expected to contribute significantly to the π-electron delocalization.[3] The combination of conjugated ligands, electron-rich metal centers, and the high degree of covalence inherent in soft-soft bonding can promote low-energy electronic interactions between the metal and the ligand. Our recent interest has been focused on novel electroactive metal-organic complexes.[4] Our current interest in d^8 thienyl complexes[5] stems from their geometric directionality and conductive potential[6] upon polymerization. Recently, we have extended this study to the construction of N- and P-bridged transition metal thienyl complexes. The simplest way to achieve this is through the introduction of a bridging co-ligand, or spacer. A non-thienyl spacer would bring an extra dimension of functionality to the complex. This paper describes a combined use of thienyl and nitrogen-containing heterocyclic ligands (depicted below) in the assembly of multimeric bifunctional d^8 networks based on a readily synthesized precursor. Introduction of different N-ligands, viz. pyridine or pyrazine-based heterocycles enables us to tune the spatial and structural features that have a direct impact on the electrochemical responses.

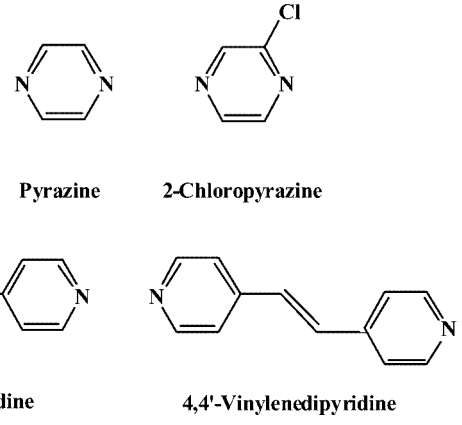

Results and Discussion

(1) Synthesis

The reaction in acetonitrile solution between equimolar *trans*-[PtBr(PPh_3)$_2$(2-thienyl)][7,8] and $AgBF_4$, gives *trans*-[Pt(MeCN)(PPh_3)$_2$(2-thienyl)]BF_4, (**1**). Its quantitative yield

[a] Department of Chemistry, Faculty of Science, National University of Singapore,
3 Science Drive 3, Singapore 117543, Singapore
Fax: (internat.) +65-6779-1691
E-mail: andyhor@nus.edu.sg

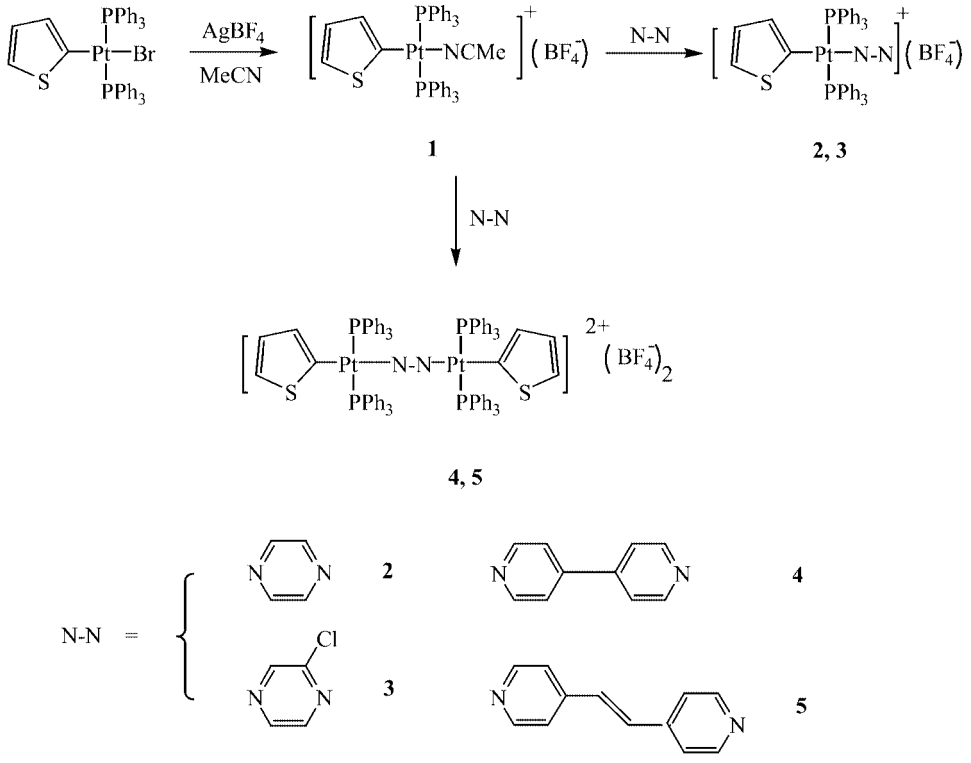

Scheme 1. Formation pathway of complexes **1**−**5**

and the presence of a labile MeCN solvent molecule make it a suitable precursor to bifunctional complexes. Although **1** can be isolated, it is more convenient to use it in situ. Upon removal of AgBr by filtration from the product mixture, addition of 4,4′-bipyridine or 4,4′-vinylenedipyridine gives dinuclear *trans,trans*-$[Pt_2(PPh_3)_4(\mu\text{-}N\text{-}N)(2\text{-thienyl})_2][BF_4]_2$ [*N*-*N* = 4,4′-bipyridine (**4**), 4,4′-vinylenedipyridine (**5**)] respectively. However, use of pyrazine and 2-chloropyrazine as substrates gives only mononuclear *trans*-$[Pt(PPh_3)_2(\eta^1\text{-}N\text{-}N)(2\text{-thienyl})][BF_4]$ [*N*-*N* = pyrazine, (**2**), 2-chloropyrazine, (**3**)] as yellow solids in high yields, despite the presence of a *trans*-disposed N-functionality (Scheme 1).

These illustrate an effective nuclear selectivity through a simple control of the N-spacer. Heterocycles in which charge delocalization is efficient, such as **2** and **3**, would have a lower nucleophilicity of the second nitrogen to an extent that it prefers to be pendant rather than bridging. The presence of the bulky PPh_3 ligand could also impede the approach of the neighboring Pt^{II} moiety towards a less protruded heterocyclic arm. Construction of cationic metal-based molecular boxes have met with a similar fate.[9,10] NMR analysis suggested that these cationic complexes are nonlabile. The ^1H coordination shifts (upfield) of the α- and β- pyrazine or pyridine hydrogen atoms (possibly due to shielding by the PPh_3 ligand) are indicative of coordinative nonlability. The α- and β-pyridine hydrogen atoms of **2** are similarly shifted upfield to δ = 8.21, 7.96 ppm, relative to free pyrazine (δ_H = 8.58), and, similarly for **5**, to δ = 7.81, 7.06 ppm, relative to free 4,4′-vinylenedipyridine (H_α δ = 8.62, H_β δ = 8.39 ppm). The ^{31}P NMR spectra of all the complexes showed the expected *trans*-phosphanes [typically $^1J_{Pt\text{-}P}$ (ca. 3480 Hz)] that are equivalent. As expected, both the shifts and couplings are fairly insensitive to subtle electronic changes in the *cis* N-ligands.

(2) Solid State Structures

Complexes **3** (Figure 1) and **5** (Figure 2) were chosen as models for X-ray crystallographic elucidation of the solid-state structures. The refinement data and bond/angle parameters are collected in Table 1 and Table 2, respectively. Complex **3** is mononuclear, comprising two *trans*-oriented phosphanes [P(2)−Pt(1)−P(2) 176.28(6)°] and a thienyl

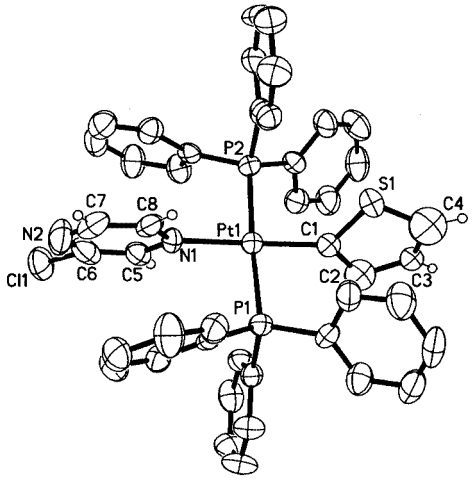

Figure 1. Thermal ellipsoids (50% probability) of **3** with the atomic numbering scheme

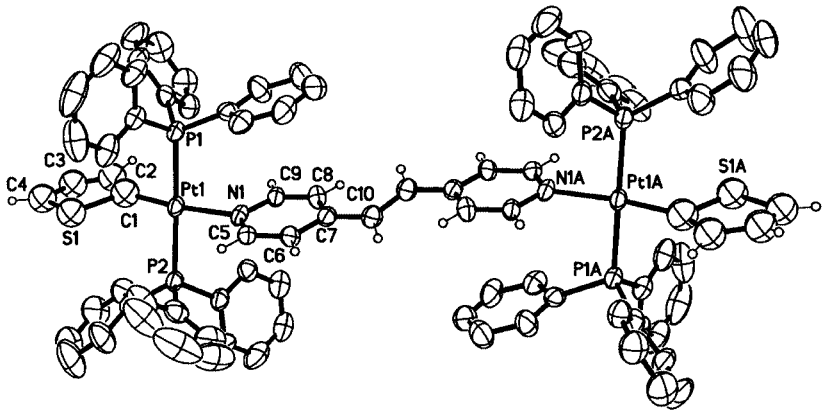

Figure 2. Thermal ellipsoids (50% probability) of **5** with the atomic numbering scheme

Table 1. Crystallographic data and structure refinement details for **3** and **5**

Complex	**3**	**5**
Empirical formula	$C_{45}H_{38}BCl_3F_4N_2P_2PtS$	$C_{92}H_{80}B_2F_8N_2O_3P_4Pt_2S_2{\cdot}CH_2Cl_2$
Formula mass	1089.02	2100.33
Color	pale yellow	yellow
Crystal size (mm)	0.26 × 0.14 × 0.10	0.28 × 0.15 × 0. 06
Crystal system	tetragonal	monoclinic
Space group	*P*4(3)	*P*2/*c*
T (K)	295(2)	223(2)
a (Å)	10.6753(5)	22.654(3)
b (Å)	10.6753(5)	11.2330(13)
c (Å)	38.654(3)	20.113(2)
α (°)	90	90
β (°)	90	111.021(2)
γ (°)	90	90
F(000)	2156	2084
V (Å^3)	4405.1(4)	4777.5(10)
Z	4	2
Absorption coefficient (mm^{-1})	3.540	3.154
Density (g·cm^{-3})	1.644	1.459
Index ranges	$-12 \le h \le 10$, $-12 \le k \le 12$, $-45 \le l \le 45$	$-26 \le h \le 26$, $-12 \le k \le 13$, $-23 \le l \le 23$
Reflections collected	25879	26547
Independent reflections	7761(R_{int} = 0.0636)	8416 (R_{int} = 0.0515)
Final *R* indices [$I > 2\sigma(I)$]	R_1 = 0.0423, wR_2 = 0.0548	R_1 = 0.0563, wR_2 = 0.1570
R indices (all data)	R_1 = 0.0546, wR_2 = 0.0565	R_1 = 0.0818, wR_2 = 0.1683
Goodness-of-fit on F^2	0.995	1.043
Largest diff. peak and hole (e·Å^{-3})	1.141 and −0.889	3.154 and −1.813

group opposite the chloropyrazine ring [N(1)−Pt(1)−C(1) 179.4(5)°]. The nitrogen atom meta to the chloro functionality is preferentially coordinated whereas the ortho counterpart is pendant. The thienyl and chloropyrazine rings are tilted at an angle of 29.5° to each other. The proximity of the phenyl rings makes the pendant nitrogen atom less susceptible to attack. Complex **5** is dinuclear with a 4,4′-vinylenedipyridine group bridging two Pt^{II} centers, opposite two thienyl terminal ligands [N(1)−Pt(1)−C(1) 168.9(2)°]. The two pyridyl rings are strictly coplanar (θ, 0°).

Complex **3** has a noncrystallographic twofold symmetry along the N(1)−Pt(1)−C(1) axis. Both substituents at the Pt(1) center, namely thienyl and 2-chloropyrazine groups are disordered along this axis. Complex **5** has a center of inversion between the methylene carbon atoms of the 4,4′-vinylenedipyridine bridging ligand, and the thienyl groups are disordered.

All Pt−N[11] [2.082(4)-2.107(4) Å] and Pt−P[10] lengths [2.3212(19)-2.323(3) Å] are normal although the Pt−N bonds of **5** are somewhat longer (in 1.2%) than in **3**. There is no evidence of perturbance to the olefinic [C(10)−C(10A) 1.352 Å] moiety at the center of the bridge.

(3) ESMS Characterization

The development of electrospray mass spectrometry (ESMS) by Fenn[12] and others[13] has provided a powerful soft technique to study multiply-charged ions, primarily large biomolecules, in solution. Recently, we have extended this development as a combinatorial-like technique to probe the chemistry of $[Pt_2(\mu\text{-}X)_2(PPh_3)_4]$ (X = S, Se).[14] In this paper we use ESMS to investigate the fragmentation of the

Table 2. Selected bond lengths and angles for **3** and **5**

3 Bond lengths (Å)			
Pt(1)−C(1)	2.005(10)	Pt(1)−P(2)	2.323(2)
Pt(1)−N(1)	2.082(4)	Pt(1)−P(1)	2.323(2)
C(4)−S(1)	1.657(14)	C(1)−S(1)	1.705(12)
C(8)−N(1)	1.316(11)	C(5)−N(1)	1.346(10)
Bond angles (°)			
C(1′)−Pt(1)−C(1)	0.8(19)	C(1)−Pt(1)−P(2)	88.2(8)
C(1)−Pt(1)−N(1)	179.4(5)	C(1)−Pt(1)−P(1)	88.1(8)
N(1)−Pt(1)−P(2)	91.60(19)	N(1)−Pt(1)−P(1)	92.12(19)
P(2)−Pt(1)−P(1)	176.28(6)		
5 Bond lengths (Å)			
Pt(1)−C(1)	2.038(7)	Pt(1)−P(2)	2.3221(19)
Pt(1)−N(1)	2.107(4)	Pt(1)−P(1)	2.3212(19)
C(4)−S(1)	1.7997(10)	C(1)−S(1)	1.7995(10)
C(9)−N(1)	1.377(8)	C(5)−N(1)	1.348(9)
C(10)-C(10A)	1.352		
Bond angles (°)			
C(1′)−Pt(1)−C(1)	11.03(17)	C(1)−Pt(1)−P(2)	94.1(2)
C(1)−Pt(1)−N(1)	168.9(2)	C(1)−Pt(1)−P(1)	87.4(2)
N(1)−Pt(1)−P(2)	89.23(16)	N(1)−Pt(1)−P(1)	90.10(16)
P(2)−Pt(1)−P(1)	175.73(7)		

parent ions in solution. Analysis of the mononuclear complexes in CH_2Cl_2 in the positive ion mode gave a $[M(N\text{-}N)]^+$ peak for **2** (m/z = 881.7) and **3** (m/z = 915.7) [M = $Pt(PPh_3)_2$(2-thienyl); *N*-*N* = pyrazine, (**2**), 2-chloropyrazine, (**3**)]. In these complexes, there is a common peak associated with the replacement of the pyrazine ligand by MeCN viz. $[M(MeCN)]^+$ (m/z = 843.8), which was observed as the main peak for complex **1**. These data suggested that the solid-state identity of these complexes is maintained in solution.

The positive-ion ES mass spectrum of complex **5** dissolved in CH_2Cl_2 is shown in Figure 3. A possible fragmentation pathway is illustrated in Scheme 2. The presence of the intact, doubly charged molecular ion Peak A (m/z = 892.7, 100%), $[M_2(4,4'\text{-vinylenedipyridine})]^{2+}$ lends support to the suggestion that the solution and solid state structures are in agreement. Fragmentation peaks B (m/z = 802.0, 10%), D (m/z = 843.8, 4%), and C (m/z = 983.8, 32%) were also detected, corresponding to M^+, $[M(MeCN)]^+$ and $[M(4,4'\text{-vinylenedipyridine})]^+$, respectively. Similarly, in the positive-ion ES mass spectrum of complex **4**, the intact, doubly charged molecular ion peak at m/z = 880.1 was observed, together with the fragmental molecular ion peaks at m/z = 957.0 {$[M(4,4'\text{-bipyridine})]^+$}, 802.0 and 843.8.

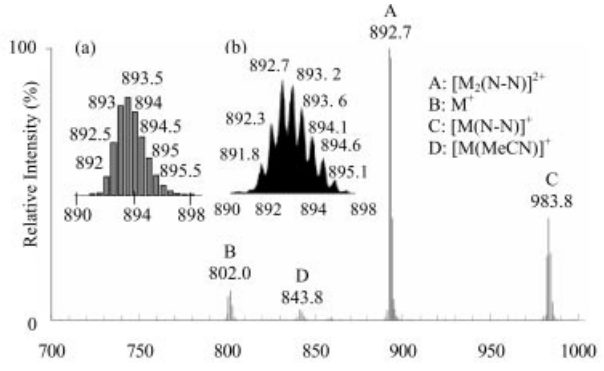

Figure 3. Positive-ion ES mass spectrum of **5** in CH_2Cl_2 solvent. The insets show the (a) calculated and (b) observed isotope distribution pattern for the intact dinuclear parent ion

Their formation can be explained by bridge cleavage by the residual MeCN molecule, thereby generating two cationic mononuclear complexes in which one bears a pendant heterocyclic ligand and the other captures the solvent ligand (Scheme 2). The ligand replacement or bridge cleavage by the strong coordination solvent MeCN has been reported before.[15] However, we should add that this takes place only when voltage is applied under spectrometric conditions. The cleavage invariably occurs at the heterocyclic junction, indicating that this is the weakest link in this series of bifunctional networks. The strong σ-donating and π-accepting character of the phosphanes as well as the anionic nature of thienyl, which electrostatically strengthens the M−C bond, make them relatively immune to such attack.

(4) Electrochemical Behavior

Cyclic voltammetric (CV) studies were performed on complexes **2**, **3**, **4** and **5** (1 mM) in CH_2Cl_2 by using Bu_4NBF_4 (0.10 M) as the supporting electrolyte. All complexes show one irreversible oxidation wave in the first scan. Complexes **4** and **5** show different electrochemical behavior from that of **2** and **3**. The repetitive cycling profiles for **5** are illustrated in Figure 4.

During the first cycle, the forward (anodic) scan gave a complex oxidation wave $\mathbf{O_1}$, which could be assigned to thiophene oxidation,[16] with at least two unresolved peaks. On reversing the scan, the reduction peaks $\mathbf{R_3}$ and $\mathbf{R_2}$ were observed. During the second cycle, new oxidation peaks $\mathbf{O_2}$ and $\mathbf{O_3}$ emerged, which were not observed on the first scan. Associated with these, the earlier oxidation wave $\mathbf{O_1}$ dropped significantly in the second anodic scan, and disappeared completely in subsequent cycles. Conversely, peaks $\mathbf{O_2/R_2}$ and $\mathbf{O_3/R_3}$ continued to increase in size to the tenth cycle, after which they began to decay with further cycles. This behavior is consistent with the formation of electroactive or conductive polymers or high oligomers.[17] Since these species are less readily soluble in the analyte solution, their formation would alter the redox pattern of the sample, and eventually render the analyte featureless in the CV scans. Polymerization is likely to take place at the thienyl site since electropolymerization of thiophene, bithiophene and substituted thiophenes is common.[18] When the electrode was removed from solution at the conclusion of the scanning experiments, rinsed with CH_2Cl_2 and dried, a greenish thin film was visible on the electrode surface. The

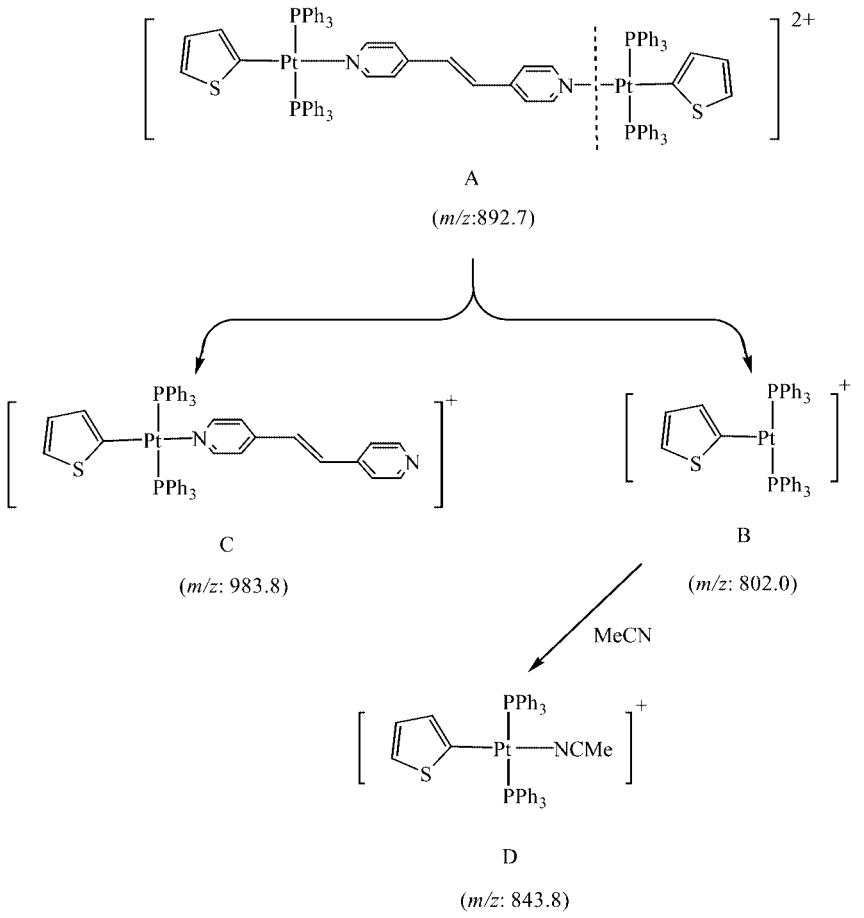

Scheme 2. Possible fragmentation pathway of **5** depicting the species observed in the positive ion ES mass spectrum

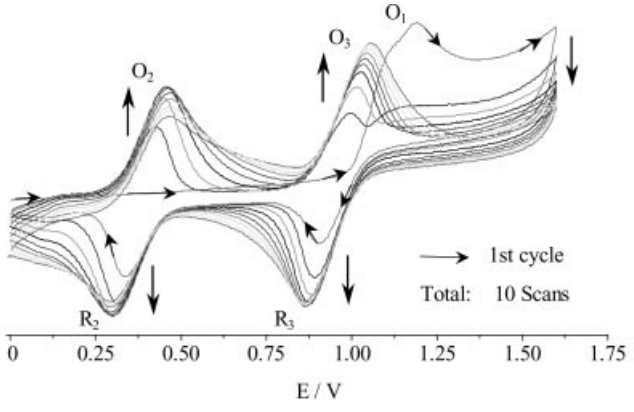

Figure 4. Continuous cyclic scanning between 0.00 to +1.60 V of **5** (0.1 mol·dm^{-3}) supported by Bu_4NBF_4 in CH_2Cl_2

material properties of this film are under investigation in our laboratory.

Cycling experiments on **4** revealed a similar decay phenomenon, with slightly different redox potentials. This suggests that the CV behavior is structurally related, and the redox potentials are sensitive to the bridging ligands. Accordingly, **2** and **3**, which are isostructural, show similar initial oxidative behavior to that of **4** and **5** (i.e. only a broad, irreversible oxidation wave) but no corresponding film formation is observed with continuous cycling. Cycling of these two analyte solutions resulted in the decrease of the oxidation wave $\mathbf{O_1}$ with no other obvious peak formation. The relevant electrochemical parameters for the complexes are summarized in Table 3. The CV profiles thus serve as supporting finger-printing diagnosis for these complexes.

In an attempt to understand this disparity, we carried out further electrochemical investigations of the films. After film formation (typically 10 scans), the potential cycling in the complex solution was terminated, and the film-coated electrode was washed with CH_2Cl_2. The electrode was then re-immersed in the blank electrolyte solution and cycled again between +0.00 V and +1.60 V. The peak heights decreased slowly with repetitive potential cycling, suggesting that the films formed from **4** and **5** are not electrochemically stable. The CV responses of these films upon treatment are also different from those seen in the $\mathbf{O_2/R_2}$ and $\mathbf{O_3/R_3}$ couples when the films were first formed. As seen in Table 3, after the tenth cycle, the anodic peak current in $\mathbf{O_2}$ is 2.79 $\times$ 10^{-5} A (i_{pc}^{R2}/i_{pa}^{O2} = 0.96 in this cycle) while that in $\mathbf{O_3}$ is 3.68 $\times$ 10^{-5} A (i_{pc}^{R3}/i_{pa}^{O3} = 1.02). This gives an $\mathbf{O_2/O_3}$ peak height ratio of 0.76. Similar analysis of the isolated film (Figure 5) shows 9.57 $\times$ 10^{-6} A for the anodic peak current in $\mathbf{O_2}$ and 1.58 $\times$ 10^{-5} A for that in $\mathbf{O_3}$, thus yielding a ratio of 0.60 (i_{pc}^{R2}/i_{pa}^{O2} = 0.86 and i_{pc}^{R3}/i_{pa}^{O3} = 0.73). The current after film formation and isolation is unusual but can be understood. Firstly, the electrogenerated cation could be a very reactive electrophilic Pt^{III}, which is

Table 3. Electrochemical data for complexes **2**−**5** and films formed at a glassy carbon electrode

Complex[a]	E_{pa}^{O1}[b]	E_{pc}^{R3}[c]	E_{pa}^{O3}	$\Delta E_{pp(3)}$[d]	i_{pc}^{R3}/i_{pa}^{O3}[e]	E_{pc}^{R2}	E_{pc}^{O2}	$\Delta E_{pp(2)}$	i_{pc}^{R2}/i_{pa}^{O2}
2	1.26	–	–	–	–	–	–	–	–
3	1.20	–	–	–	–	–	–	–	–
4	1.16	0.91	–	–	–	0.33	–	–	–
5	1.28	0.90	–	–	–	0.31	–	–	–
Film (**4**)[f]	–	0.86	1.11	0.25	0.95	0.26	0.52	0.26	0.94
Film (**5**)[g]	–	0.82	1.12	0.30	1.02	0.25	0.51	0.26	0.96

[a] Electrochemical data for complexes **2**−**5** from cyclic voltammetry in CH_2Cl_2/0.1 M Bu_4NBF_4: potential in V vs. $Ag/AgNO_3$, scan rate 100 mV s^{-1}. [b] Anodic peak potential for irreversible oxidation. [c] Cathodic peak potential for reduction. [d] Peak-to-peak separation $\Delta E_{pp} = E_{pa} - E_{pc}$ (V). [e] The ratio of reduction current to oxidation current. [f] Film (**4**) was derived from 10 cycles of **4**. [g] Film (**5**) was derived from 10 cycles of complex **5**.

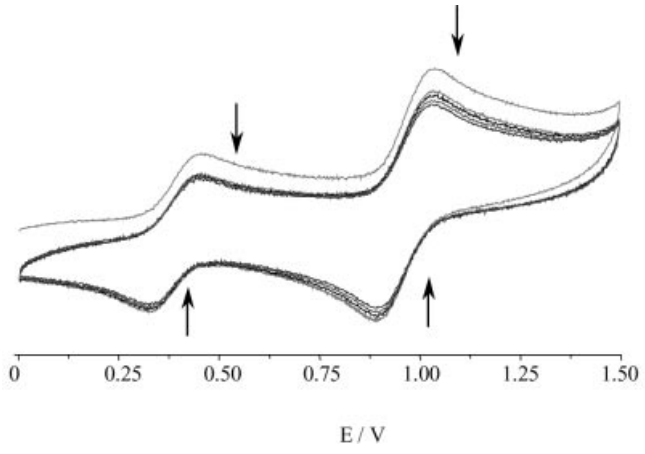

Figure 5. Continuous cyclic scanning between 0.00 to +1.60 V of the film formed from **5** in blank electrolyte solution containing 0.1 M Bu_4NBF_4 in CH_2Cl_2

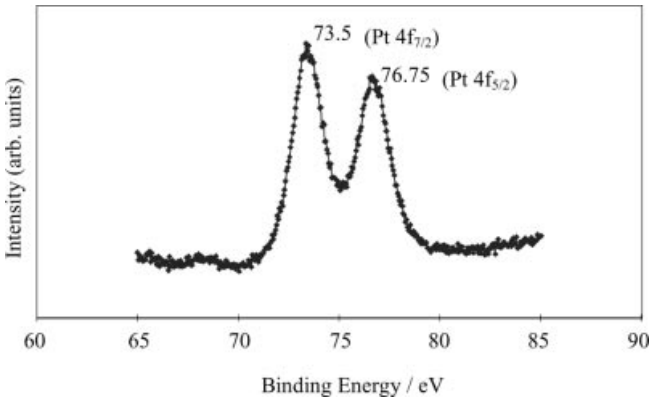

Figure 6. The XPS spectra of the film formed from **5**

bound to decay rapidly at room temperature.[19] Secondly, the stability of the film at the potentials at which it is formed could be poor, which is known as the "thiophene paradox"[20] in the synthesis of polythiophene conducting polymers via electrooxidation.

To gain some understanding of the elemental composition of the film, we carried out an XPS analysis[21] of the film formed from **5**. This film was formed typically after about 10 scans. When the potential cycling of the complex solution was terminated, the film-coated electrode was retrieved and washed with CH_2Cl_2, and the film analyzed by XPS, the Pt(4f) spectrum showed the spin-orbit components separated by 3.25 eV (Figure 6). The Pt(4f) binding energies, which compare well with those of phosphane-bearing platinum,[22] are indicative of Pt^{II}. Further S(2p), N(1s) and P(2p) spectral analyses revealed fairly typical spectra for thienyl, bipyridyl and phosphane complexes. Further studies of the film properties and characteristics, which are outside the present scope, will be a subject of our future reports.

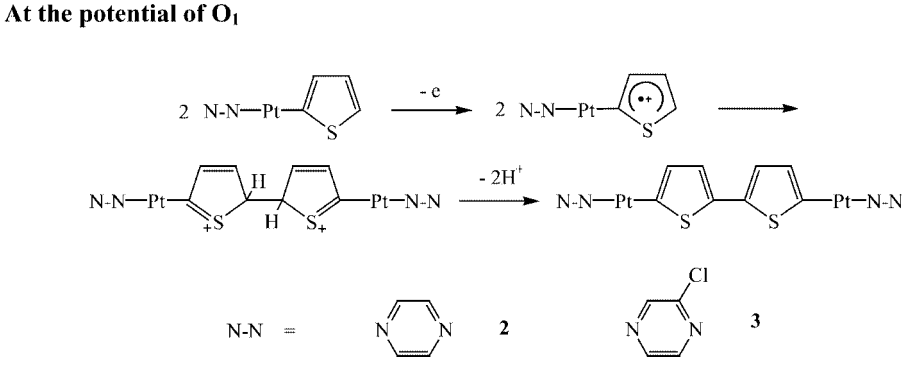

Scheme 3. Possible dimerization pathway for the mononuclear species **2** and **3** under applied potential in CV experiments

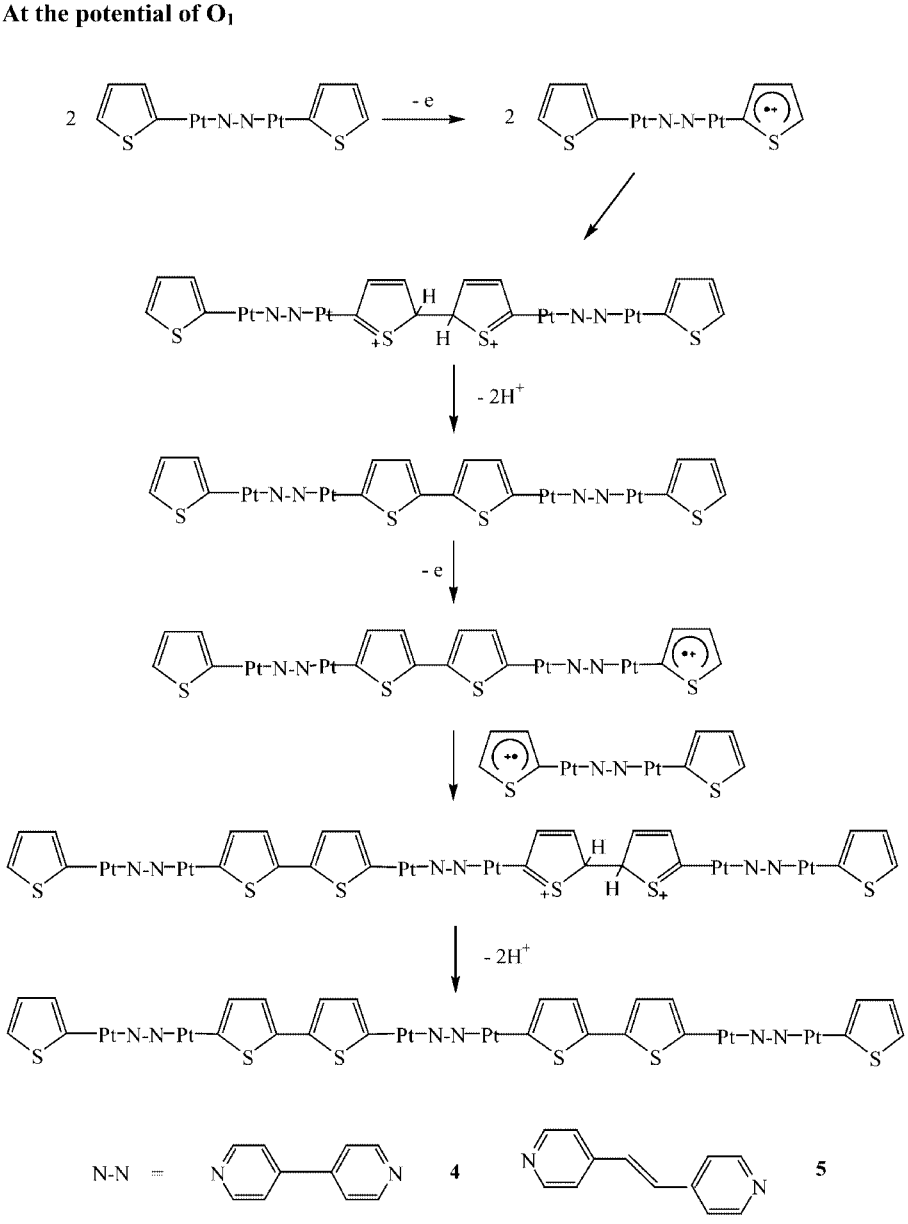

Scheme 4. Possible polymerization process for **4** and **5** that leads to film formation on the surface of the electrode from continuous scanning

It is not our primary interest to study the details of the electropolymerization mechanism, but we can propose a reasonable pathway, involving repetitive electrogeneration of a cation radical, followed by α-α coupling, that is grounded in the literature[23−25] and allows us to explain the different behavior of the mono- (Scheme 3) and dinuclear complexes (Scheme 4). At the first cycle of electropromoted coupling, the dinuclear precursors **4** and **5** yield bithiophene-bridged Pt_4 complexes that have two free ends of α-thienyl group. The latter could undergo further coupling using the free α functionality by a similar mechanism as above. This would transform a Pt_4 into a Pt_6 chain, and so on. As there is no facile chain-termination step, a film would be the obvious product on ending the electropolymerization cycles. However, for mononuclear complexes **2** and **3**, dimerization would lead to a Pt_2 complex bridged through bithiophenyl groups and with terminal N−N groups. There is no α-thienyl end and hence no further thienyl−thienyl coupling. These electrogenerated dinuclear complexes are soluble and they do not lead to further polymerization or film formation.

Conclusion

Using ESMS as a guide, we have successfully constructed novel mononuclear and dinuclear thienylplatinum complexes with different bridging coligands. The nuclear selectivity can be easily controlled by the choice of the N-spacer. The electrochemical experiments led to promising metal-

containing thin films from electrocycling of dinuclear complexes with a thiophene function at either end. The potential for film formation from structurally characterizable materials and the possibility for adjusting the film properties through the use of different spacers would add a new dimension to our current research.

Experimental Section

All reactions were routinely performed under purified nitrogen using standard Schlenk techniques. Solvents used were of reagent grade and were freshly distilled and degassed under purified nitrogen before use. Elemental analyses were carried out in the Chemistry Department of National University of Singapore (NUS). ^{1}H and ^{31}P NMR spectra were recorded on a Bruker ACF 300 MHz spectrometer at ca. 300 K. ^{1}H and ^{31}P NMR chemical shifts are quoted in ppm downfield of Me_4Si and externally referenced to 85% H_3PO_4, respectively.

Electrospray Mass Spectrometry (ESMS): The electrospray mass spectra were recorded in positive-ion mode on a Finningan LCQ spectrometer. The spray voltage was 4.5 kV, and the capillary temperature was 40 °C. The peaks in the ESMS are identified by the most intense *m*/*z* value within the isotopic mass distribution. Isotope patterns were recorded under high-resolution conditions for all major ions and compared with theoretical patterns obtained using the Isotope program.[26] In all cases there was good agreement between the experimental and calculated isotopic mass distributions.

Cyclic Voltammetry (CV): Containers (glassware, polyethylene bottles, etc.) were soaked overnight in 10% HNO_3 prior to use. Electrochemical experiments were performed with an Autolab PGSTAT 30 electrochemical system (Eco Chemie, Netherlands). A locally made three-electrode glass cell of approximately 5 mL capacity was used for all electrochemical experiments. The reference electrode (Ag|$AgNO_3$, 0.01 M in MeCN) was placed in a compartment containing the supporting electrolyte solution separated from the working electrode compartment by a 4 mm diameter Vycor frit. Working electrodes were 3 mm diameter glassy carbon disks.

***trans*-[Pt(PPh$_3$)$_2$(pyrazine)(2-thienyl)][BF$_4$] (2):** To a stirred solution of $AgBF_4$ (19.5 mg, 0.1 mmol) in MeCN (2 mL) was added a solution of [*trans*-PtBr(PPh$_3$)$_2$(2-thienyl)] [88.3 mg, 0.1 mmol in CH_2Cl_2 (10 mL)]. The mixture was stirred, shielded from light, for 1 h and AgBr was removed by filtration. A solution of pyrazine (8.0 g, 0.1 mmol) in CH_2Cl_2 (2 mL) was then added to the colorless filtrate. The mixture was stirred at room temperature for 4 h. The clear pale yellow solution was condensed to about 2 mL under vacuum, and the pale yellow solid residue of complex **2** (92.0 mg, 95%) was collected by adding Et_2O. The product was purified by recrystallization from CH_2Cl_2/hexane to give pale yellow crystals. $C_{44}H_{37}BF_4N_2P_2PtS$ (969.69): calcd. C 54.5, H 3.85, N 2.89, S 3.30; found C 54.38, H 3.59, N 2.85, S 3.51. ^{1}H NMR ($CDCl_3$): δ = 7.2−7.5 (m, 60 H, phenyl), 8.21 (d, 1 H, pyrazine), 7.96 (d, 1 H, pyrazine), 6.93 (d, 1 H, thiophene), 6.37 (t, 1 H, thienyl), 5.94 (d, 1 H, thienyl) ppm. ^{31}P NMR ($CDCl_3$): δ = 18.34 (s) ppm.

***trans*-[Pt(2-chloropyrazine)(PPh$_3$)$_2$(2-thienyl)][BF$_4$] (3):** The synthesis follows that of **2**. 2-Chloropyrazine (11.5 mg, 0.1 mmol) and [*trans*-PtBr(2-thienyl)(PPh$_3$)$_2$] (88 mg, 0.1 mmol) gave a light yellow powder of complex **3** (98.8 mg, 94%). Recrystallization from CH_2Cl_2/Et_2O gave light yellow crystals. $C_{44}H_{36}BClF_4N_2P_2PtS$ (1004.13): calcd. C 52.63, H 3.61, N 2.79, S 3.19; found C 52.28, H 3.12, N 2.55, S 3.58. ^{1}H NMR ($CDCl_3$): δ = 7.2−7.5 (m, 60 H, phenyl), 8.69 (d, 1 H, pyrazine), 7.93 (d, 1 H, pyrazine), 7.61 (s, 1 H, pyrazine), 6.94 (d, 1 H, thiophene), 6.39 (t, 1 H, thiophene), 5.96 (d, 1 H, thiophene) ppm. ^{31}P NMR ($CDCl_3$): δ = 18.12 (s) ppm.

***trans,trans*-[Pt$_2$(μ-4,4′-bipyridine)(PPh$_3$)$_4$(2-thienyl)$_2$][BF$_4$]$_2$ (4):** The synthetic procedure is similar to that of **2**. 4,4′-Bipyridine (7.8 mg, 0.05 mmol) and complex [*trans*-PtBr(2-thienyl)(PPh$_3$)$_2$] (88 mg, 0.1 mmol) gave a pale yellow solid residue of complex **4** (78.5 mg, 80%). $C_{90}H_{74}B_2F_8N_2P_4Pt_2S_2$ (1935.38): calcd. C 55.85, H 3.85, N 1.45, S 3.31; found C 55.40, H 3.79, N 1.38, S 3.83. ^{1}H NMR (MeCN): δ = 7.2−7.5 (m, 60 H, phenyl), 8.48 (d, 4 H, pyridine), 6.89 (d, 4 H, pyridine), 7.03 (d, 2 H, thiophene), 6.35 (t, 2 H, thiophene), 5.37 (d, 2 H, thiophene) ppm. ^{31}P NMR (MeCN): δ = 18.46 (s) ppm.

***trans,trans*-[Pt$_2$(PPh$_3$)$_4$(2-thienyl)$_2$(μ-4,4′-vinylenedipyridine)][BF$_4$]$_2$ (5):** The procedure is similar to that of **2**. 4,4′-Vinylenedipyridine (9.1 mg, 0.05 mmol) and complex [*trans*-PtBr(2-thienyl)(PPh$_3$)$_2$] (88 mg, 0.1 mmol) gave a yellow solid residue of complex **5** (80.3 mg, 82%). Recrystallization from CH_2Cl_2/hexane gave pale yellow crystals. $C_{92}H_{76}B_2F_8N_2P_4Pt_2S_2$ (1961.42): calcd. C 56.34, H 3.91, N 1.43, S 3.27; found C 56.49, H 3.65, N 1.50, S 3.16. ^{1}H NMR ($CDCl_3$): δ = 7.2−7.5 (m, 60 H, phenyl), 7.81 (d, 4 H, pyridine), 7.06 (d, 4 H, pyridine), 7.07 (s, 2 H, pyridine), 6.96 (d, 2 H, thiophene), 6.41 (t, 2 H, thiophene), 5.97 (d, 2 H, thiophene) ppm. ^{31}P NMR ($CDCl_3$): δ = 18.59 (s) ppm.

Crystallography: The diffraction experiments for complexes **3** and **5** were carried out on a Bruker AXS CCD diffractometer with a Mo-K_α sealed tube. The software SMART[27] was used for collecting frames of data, indexing reflections, and determination of lattice parameters, SAINT[27] for integration of intensity of reflections and scaling, SADABS[28] for empirical absorption correction, and SHELXTL[29] for space group and structure determination, refinements, graphics, and structure reporting. In the crystal structures of **3** and **5**, the thienyl groups were disordered. Two independent models were refined in each case. The chlorine atom of the chloropyrazine ligand in **3** was also found to be disordered. The asymmetric unit in **5** has half a dichloromethane solvate molecule and 1.5 mol of disordered water molecules. The positive residual electron densities in **5** were associated with the Pt atom. A summary of crystallographic parameters for the data collections and refinements is given in Table 1. CCDC-182455 and CCDC-182456 contain the supplementary crystallographic data for this paper. These data can be obtained free of charge at www.ccdc.cam.ac.uk/conts/retrieving.html [or from the Cambridge Crystallographic Data Centre, 12, Union Road, Cambridge CB2 1EZ, UK; Fax: (internat.) + 44-1223/336-033; E-mail: deposit@ccdc.cam.ac.uk].

Acknowledgments

The authors acknowledge the National University of Singapore (NUS) for financial support and the technical staff for supporting services, in particular, J. J. Vittal and G. K. Tan for the valuable help in crystallographic analysis and interest in the project, L. J. Chen for spectroscopic assistance, and H. Xu for XPS (NUS Physics) assistance. F. Z. thanks NUS for the research scholarship. X. Xu thanks NUS for a postdoctoral fellowship. We also thank W. Henderson (Waikato) for helpful discussions and advice, and P. Teo for some experimental assistance.

[1] J.-M. Lehn, *Supramolecular Chemistry: Concepts and Perspectives*, VCH, Weinheim, **1995**, 139−160.

[2] [2a] M. Schweiger, S. R. Seidel, A. M. Arif, P. J. Stang, *Angew. Chem. Int. Ed.* **2001**, *40*, 3467−3469. [2b] S. Leininger, B. Olenyuk, P. J. Stang, *Chem. Rev.* **2000**, *100*, 853−908. [2c] M. Fujita, *Chem. Soc. Rev.* **1998**, 27, 417−425. [2d] B. Olenyuk, J. A. Whiteford, A. Fechtenkötter, P. J. Stang, *Nature* **1999**, *398*, 796−799.
[3] R. D. Markwell, I. S. Butler, A. K. Kakkar, M. S. Khan, Z. H. Al-Zakwani, J. Lewis, *Organometallics* **1996**, *15*, 2331−2337.
[4] X. Xu, S. W. A. Fong, Z. H. Li, Z. H. Loh, F. Zhao, J. J. Vittal, W. Henderson, S. B. Khoo, T. S. A. Hor, *Inorg. Chem.* **2002**, *41*, 6838−6845.
[5] Y. Xie, B. M. Wu, F. Xue, S. C. Ng, T. C. W. Mak, T. S. A. Hor, *Organometallics* **1998**, *17*, 3988−3995.
[6] A. J. Heeger, *Angew. Chem. Int. Ed.* **2001**, *40*, 2591−2611.
[7] Y. Xie, B. M. Wu, F. Xue, S. C. Ng, T. C. W. Mak, T. S. A. Hor, *J. Organomet. Chem.* **1997**, *531*, 175−181.
[8] L.-Y. Chia, W. R. McWhinnie, *J. Organomet. Chem.* **1980**, *188*, 121−128.
[9] P. J. Stang, D. H. Cao, *J. Am. Chem. Soc.* **1994**, *116*, 4981−4987.
[10] P. J. Stang, D. H. Cao, S. Saito, A. M. Arif, *J. Am. Chem. Soc.* **1995**, *117*, 6273−6283.
[11] A. Albinati, F. Isaia, W. Kaufmann, C. Sorato, L. M. Venanzi, *Inorg. Chem.* **1989**, *28*, 1112−1122.
[12] [12a] J. B. Fenn, Nobel lecture, **2002**, Stockholm University. [12b]D. L. Zhan, J. B. Fenn, *Int. J. Mass. Spectrom.* **2002**, 219, 1−10. [12c] J. B. Fenn, M. Mann, C. K. Meng, S. F. Wong, C. M. Whitehouse, *Science* **1989**, *246*, 64−71;
[13] [13a] B. F. G. Johnson, J. S. McIndoe, *Coord. Chem. Rev.* **2000**, *200*, 901−932. [13b] D. P. Gallasch, E. R. T. Tiekink, L. M. Rendina, *Organometallics* **2001**, *20*, 3373−3382. [13c] W. Henderson, B. K. Nicholson, L. J. McCaffrey, *Polyhedron* **1998**, *17*, 4291−4313.
[14] [14a] J. S. L. Yeo, J. J. Vittal, T. S. A. Hor, *Eur. J. Inorg. Chem.* **2003**, 277−280. [14b] J. S. L. Yeo, J. J. Vittal, W. Henderson, S. A. Hor, *J. Chem. Soc., Dalton Trans.* **2002**, 328−336. [14c] S. -W. A. Fong, W. T. Yap, J. J. Vittal, T. S. A. Hor, W. Henderson, A. G. Oliver, C. E. F. Rickard, *J. Chem. Soc., Dalton Trans.* **2001**, 1986−2002.
[15] M. D. Levin, J. Stang, *J. Am. Chem. Soc.* **2000**, *122*, 7428−7429.
[16] B. J. Maclean, P. G. Pickup, *J. Mater. Chem.* **2001**, *11*, 1357−1363.
[17] Y. Zhu, M. O. Wolf, *Chem. Mater.* **1999**, *11*, 2995−3001.
[18] [18a] M. Satoh, K. Imanishi, K. Yoshino, *J. Electroanal. Chem.* **1991**, *317*, 139−151. [18b] J. Heinze, H. John, M. Dietrich, P. Tschuncky, *Synth. Met.* **2001**, *119*, 49−52. [18c] J. Roncali, A. Yassar, F. Garnier, *Synth. Met.* **1989**, *28*, C275−C280.
[19] A. Klein, W. Kaim, *Organometallics* **1995**, *14*, 1176−1186.
[20] B. Krische, M. Zagorska, *Synth. Met.* **1989**, *28*, C263−C268.
[21] K. G. Neoh, E. T. Kang, K. L. Tan, *J. Phys. Chem. B* **1997**, *101*, 726−731.
[22] [22a] E. de Wolf, A. J. M. Mens, O. L. J. Gijzeman, J. H. van Lenthe, L. W. Jeneskens, B.-J. Deelman, G. van Koten, *Inorg. Chem.* **2003**, *42*, 2115−2124. [22b] B. H. Aw, K. K. Looh, H. O. Chan, K. L. Tan, T. S. Andy Hor, *J. Chem. Soc., Dalton Trans.* **1994**, 3177−3182.
[23] J. Roncali, *Chem. Rev.* **1992**, *92*, 711−738.
[24] E. Genies, G. Bidan, A. F. Diaz, *J. Electroanal., Chem.* **1983**, *149*, 113.
[25] P. Audebert, J.-M. Catel, G. Le Coustumer, V. Duchenet, P. Hapiot, *J. Phys. Chem. B* **1998**, *102*, 8661−8669.
[26] L. J. Arnold, *J. Chem. Educ.* **1992**, *69*, 811−811.
[27] *SMART & SAINT Software Reference Manuals*, Version 4.0, Siemens Energy & Automation, Inc., Analytical Instrumentation, Madison, WI, **1996**.
[28] G. M. Sheldrick, *SADABS*, a Software for Empirical Absorption Correction, University of Göttingen, **1996**.
[29] G. M. Sheldrick, *SHELXTL*, Version 5.03, Siemens Energy and Automation Inc., Analytical Instrumentation, Madison, WI, **1996**.

Received May 28, 2003
Early View Article
Published Online October 23, 2003

